Advances in Science and Technology Research Journal

Advances in Science and Technology Research Journal, 2026, 20(10), 180–192
https://doi.org/10.12913/22998624/224724
ISSN 2299-8624, License CC-BY 4.0

Received: 2026.05.15
Accepted: 2026.07.18
Published: 2026.09.01

Numerical analysis and experimental tests of the composite-made structure of the jet-propelled aerial target

Łukasz Kiszkowiak[1], Michał Jędrak[1*], Piotr Zalewski[1]

[1] Faculty of Mechatronics, Armament and Aerospace, Military University of Technology, ul. Kaliskiego 2, 00-908 Warsaw, Poland
* Corresponding author's e-mail: michal.jedrak@wat.edu.pl

ABSTRACT

This work is the next stage of the project of an aerial target, this time related to the structural integrity of the composite-made structure of the airframe. According to aircraft design regulations, an aircraft structure must be able to support limit loads without any permanent deformation. The paper contains the methodology of determination of external loads (critical loads) of a flight envelope acting on the airframe during the flight, the numerical analysis of the strength and integrity of the airframe structure and finally ground statics tests on the measurement so-called the proof of compliance strength tests under load. The research and investigation presented are in accordance with the airworthiness regulations (CS-VLA standards) required by the European Union Aviation Safety Agency (EASA), which are prerequisite of the qualification tests of the aircraft, leading to the certification of the aircraft (type certificate). The aerial system was positively verified during the qualification tests of the system at the Polish Air Force training range and finally received the type certificate and was introduced into the service.

Keywords: aerospace engineering, unmanned aerial vehicles: composite materials, numerical analysis, ground tests.

INTRODUCTION

In 1951, the Ryan Aeronautical Company designed the Firebee, the first turbojet powered air target [1], which is used successfully to this day, and soon other designs of this type appeared on the market [2–6]. Today, reusable, turbojet powered target drones are primarily used for testing surface-to-air missile systems or training fighter pilots, but aluminium alloys of the airframe structure are generally replaced by composite materials [7–9], including the General Atomics MQ-9 family [10], the most advanced and effective UAV system. In 2013, the Polish Ministry of Defence commissioned the development of a similar system in the country. The consortium, consisting of the Air Force Institute of Technology, the MSP Szender Company, the Warsaw University of Technology, and the Military University of Technology, was selected to design and implement the project under the code "OCP-JET2 Programmable Aerial Target". The prototype set of 7 unmanned aerial vehicles (UAVs) was deployed to the Polish Armed Forces [11,12]. The system is now used to train operators of the air defence system and fighter pilots. The unmanned aerial vehicle designated "OCP-JET2", thereinafter referred to as the OCP, imitates and simulates incoming enemy combat aircraft in context of flight speed; altitude, manoeuvrability and Radar Cross Section.

The Military University of Technology, as a member of the consortium, was responsible for determining the aerodynamic properties and characteristics of the plane [13], the selection of the engine for the propulsion unit, and the monitoring system of the engine condition [14,15]. This work is the next stage of the project, this time related to the structural integrity of the OCP structure, including the numerical strength analysis and static ground tests of the aircraft frame, which is an element of the qualification tests required by the European Union Aviation Safety Agency (EASA).

The aircraft is designed in a classic aerodynamic configuration (Figure 1) with a trapezoidal wing and a T-shaped tail unit. The UAV is powered by two miniature turbine jet engines mounted in the rear part of the fuselage. The aircraft takes off from a pneumatic launcher and land on its belly or with a parachute (Figure 2). The parameters and performance of the aircraft are listed in Table 1.

The paper contains the methodology of determination of external loads (critical loads) – flight envelope, the numerical analysis of the strength of the airframe, as well as methodology and results of ground static tests. The latter, in accordance with the European airworthiness regulations (EASA), are part of the qualification tests of the aircraft, leading to the certification of the aircraft (type certificate).

MATERIALS AND METHODS

Flight envelope

The OCP aircraft designed with a take-off weight of approximately 87 kg qualifies for certification according to the European Airworthiness Regulations CS – VLA (Very Light Aircraft) [16] and the Federal Aviation Administration [17] that satisfies the following criteria: Maximum take-off weight (MTOW) of not more than 750 kg (note: MTOW is expressed in the mass unit – kg), maximum stall speed in the landing configuration (V_{S0}) of no more than 83 km/h (45 knots), approved for visual flight rules (VFR) under day conditions only.

In accordance with the CS-VLA standards, numerical calculations and ground strength tests (proof of compliance) were performed to check the airframe. According to aircraft design regulations, the aircraft structure must be able to support limit loads without any permanent deformation. At any load up to limit loads, the deformation may not interfere with safe operation. Compliance with the strength requirements of CS-VLA must be demonstrated for each critical load condition. Numerical investigations can be used, but their results must be supplemented with experimental ground static tests on the proof of compliance strength tests under load.

The first stage of the analysis is to plot the in-flight load envelope or the flight envelope [18–20]. The flight envelope of the aircraft is a graph (Figure 3) which shows the maximum values of the forces (usually the load factor, n) that act on the aircraft under different flight conditions (speeds). It is an important factor in flight and safety analysis, as it allows determining the range of permissible loads (depending on the speed and angle of attack), as well as the g-forces acting on the aircraft. The boundaries were determined according to the CS-VLA regulations for the following OCP in-flight load status (Figure 3):

1. Manoeuvring loads (in accordance with CS-VLA.333; 337).
2. Loads for specific design speeds (CS-VLA.335), such as:
   - V_A – manoeuvring speed,
   - V_C – cruising speed,
   - V_D – dive speed,
   - V_G – manoeuvring speed in inverted flight.
3. Gust loads (CS-VLA.341; VLA.333).
4. Loads in the aircraft configuration with deployed flaps (CS-VLA 345).

The characteristic points of the aircraft load envelopes are crucial for analysing the strength and safety of the aircraft under various flight conditions. Each of these points represents different

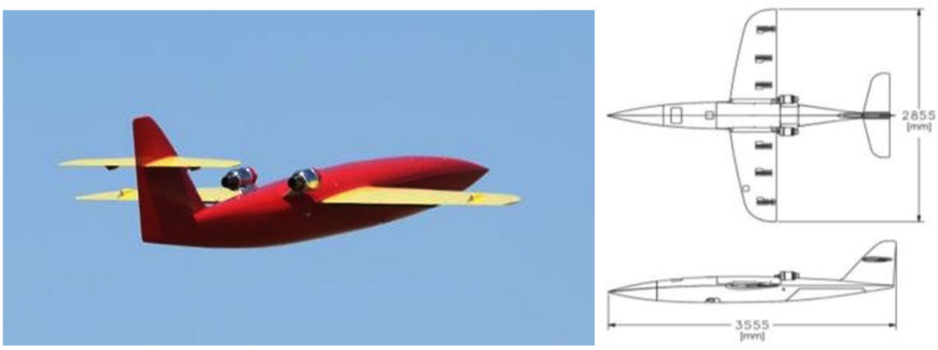

Figure 1. The OCP in flight on the left, drawing of an aircraft on the right

Figure 2. Launch of the OCP from a pneumatic launcher

Table 1. Parameters and performance of the OCP

Aircraft parameters	
Maximum take-off mass	86.6 kg
Minimum take-off mass	43.2 kg
Wing surface	1.35 m^2
Wingspan	2.85 m
Thrust of engines	2 × 160 N
Aircraft performance	
Maximum flight speed	504 km/h
Maximum ceiling	5000 m
Flight time	about 1 h
Take off: pneumatic launcher, Landing: on the belly or on a parachute	
Flight - automatic (control by autopilot), programmed according to the way points of the route. It is possible to change the route or other flight parameters during the flight in real time.	
Equipment: radar reflector to simulate the aircraft reflective surface (radar cross section)	

phases or limits that may occur during flight and play an important role in the design and operation of the aircraft. The characteristic points of the aircraft flight envelope (Figure 3) are the speeds such as: V_A,V_C,V_D and V_S – the lowest (stalling) speed at which the aircraft can maintain stability in flight, with flaps retracted, V_{SF} – the stalling speed with fully extended flaps.

In the work from the designated load envelope in the OCP flight (Figure 3), two characteristic (critical) calculation points for speed were selected due to the greatest forces and overloads. V_A= 403.45 km/h and V_D= 567.00 km/h. For these cases, an aircraft (weight W = 87 kG) achieves a positive coefficient n=10.

Numerical analysis

The numerical model was built in the SAMCEF software, which is a program used for structural analysis using the finite element method (FEM). The SAMCEF package consists of several modules that can be used independently of each other. The OCP geometry was prepared and processed using the NX 8.5 software (Unigraphics) [21–24] and then introduced to the SAMCEF program to perform numerical analyses. The aerial target geometry was obtained in the prt format , and it was a non-parametric geometry. The geometry provided was solid geometry. Interconnected surfaces were used for numerical analyses. The resulting geometry was processed to achieve consistency. To create a numerical model, it was necessary to modify the geometry to one that is recognisable and well-absorbed by the SAMCEF program.

Properly prepared geometry (Figure 4) allows for the creation of a numerical grid. The elements used to make the mesh are square elements with dimensions of 10 × 10 mm. In the numerical model, shell elements are used to map the real object (Figure 5). The number of shell elements

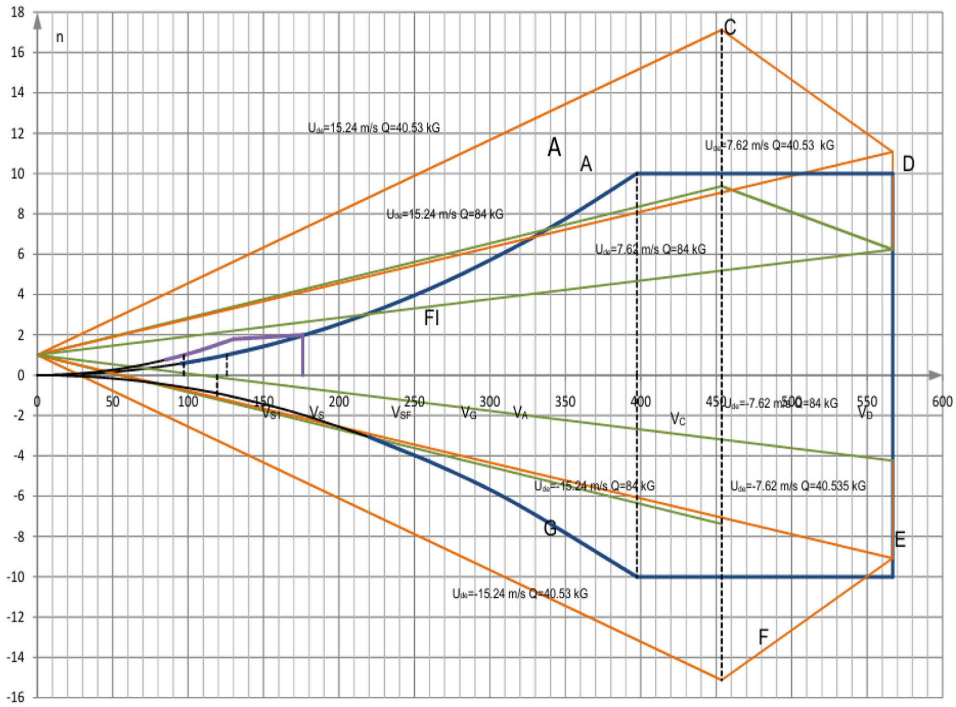

Figure 3. The OCP flight envelope. Aircraft weight: W_{max} = 84 kG; W_{min} = 40.53 kG, Load factors: manoeuvring n_{max} = 10, n_{min} = -10; from gusts n_{max} = +17.1205, n_{min} = -15.1205, Design speeds [EAS]: V_S = 127.58 km/h, V_A = 403.45 km/h, V_C = 453.6 km/h, V_D = 567 km/h, V_G = 397.44 km/h, V_{SF} = 97.56 km/h

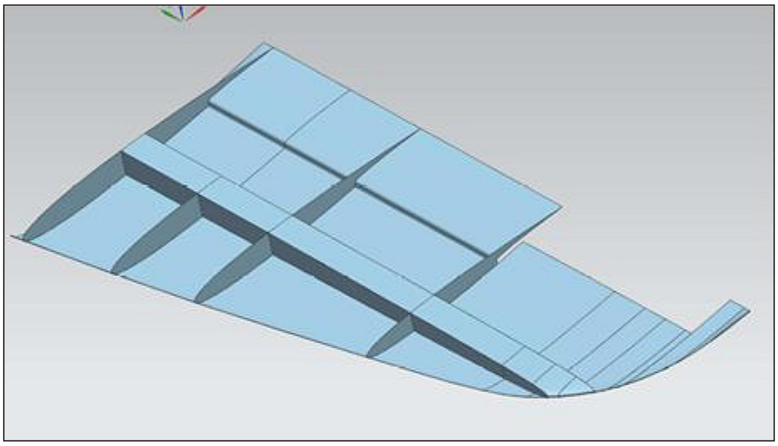

Figure 4. The CAD model of the wing geometry

from which the numerical model was built was about 30 000. A mesh convergence study was not conducted for the numerical model considered in this work, as the analysis focused primarily on qualitative trends rather than obtaining mesh-independent quantitative results. Approximately 90% of the elements were found to comply with the adopted mesh quality standards, suggesting that the generated mesh was generally suitable for the performed simulations. The remaining elements only slightly deviated from the prescribed mesh quality criteria, and their locations within the structure were not expected to have any significant influence on the numerical results.

Contemporary aircraft structures increasingly employ advanced materials in place of conventional ones, especially 2000-series aluminium alloys, due to their improved mechanical and operational properties. Carbon Fibre-Reinforced Polymer (CFRP) composites are among the most advanced materials in this category, offering high specific strength and stiffness, along with excellent resistance to corrosion and fatigue loading [25–28]. CFRP composites have become the predominant material in modern aircraft structures due to their exceptional strength-to-weight ratio, high corrosion resistance, and considerable design flexibility. These characteristics facilitate the development of lightweight, efficient, and durable aerospace components. The application of CFRP materials contributes significantly to structural weight reduction, which in turn leads to lower fuel consumption and decreased greenhouse gas emissions [29–33].

To assess the structural integrity of the composite components under static loading conditions, a composite failure criterion was employed. The structural integrity of the composite components was evaluated using the Maximum Stress failure criterion. This criterion assumes that failure initiates when any of the stress components within a laminate ply exceeds the corresponding allowable stress limit of the material. The criterion considers tensile and compressive strains in the principal material directions, as well as the in-plane shear strain.

For each ply, the calculated stress components were compared with the respective ultimate stress values provided by the material manufacturer. Failure initiation was predicted when at least one stress component reached or exceeded its allowable limit, corresponding to a failure index greater than or equal to unity. The Maximum Stress criterion provides a straightforward and computationally efficient method for assessing the onset of damage in composite laminates and is particularly suitable when strain-based material properties are available.

In the present study, the Maximum Stress criterion was employed during the static analysis to identify critical regions of the composite structure and to verify that the predicted stress levels remained below the allowable material limits under the applied loading conditions.

Connecting structural elements, such as spar, ribs, and skin was carried out using the "glue" function. The "glue" function can be used to connect two surfaces together. The "glue" operation has the same effects as a manual connection between nodes. Its main advantage is that a model does not have to be created from a single piece of geometry. Several components can be loaded and combined with the "glue" function. This is less time-consuming and simplifies the way of modelling individual parts of the aircraft. The girder belt of the air target has been divided into appropriate lengths of surfaces to facilitate the process of imparting material properties. The largest number of layers occurs in the middle part of the girder due to the largest bending moments. The other OCP structural elements were modelled based on the design documentation and the corresponding lamination schemes in the same way as the wing and its structural elements (Figure 6).

The construction materials that were used in the SAMCEF program to build the OCP numerical model of the composite structure [34–38] are shown in Tables 2–5.

The boundary conditions applied to the numerical model were defined by constraining the structure at four points located near the centre of mass on the outer surface of the fuselage, in the vicinity of the wing–fuselage attachment region. In the discrete model, support in the form of weightless rods was used to block translational displacements in selected directions (all translational degrees of freedom). In the calculation, the loads resulting from the load boundary point D are determined. They are shown in Figures 7 and 8.

The forces in the design model were applied to the nodes closest to the points of application in the actual test using a unit force expressed in

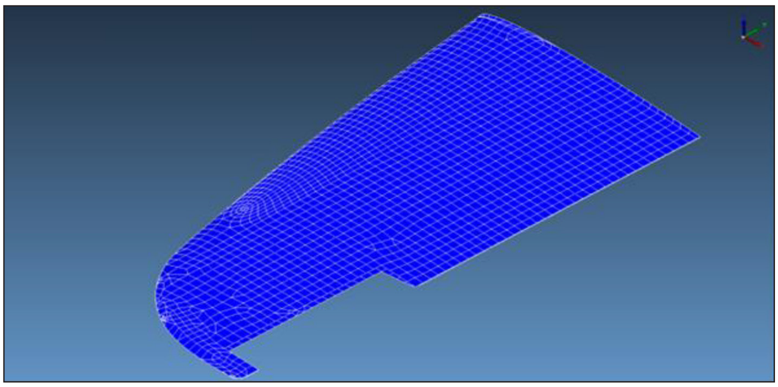

Figure 5. The FEM model of the wings

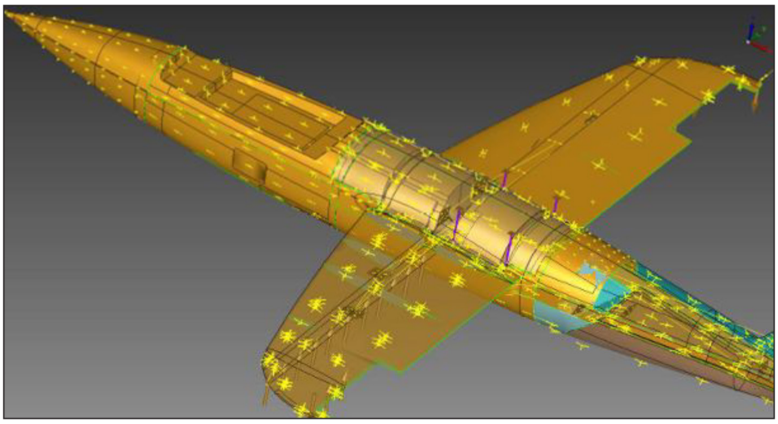

Figure 6. The FEM OCP model with defined main material axes

Table 2. Aeroglass 48 (symmetrical glass fabric with LG700 resin)

Parameter	X	Y	Z
Young modules [GPa]	18	18	10
Poisson ratio	0.22	0.22	0.22
Shear modules [GPa]	2.9	6	6
Density [kg/m^3]		1800	
Tensile strength [MPa]	300	300	65
Compressive strength [MPa]	250	250	120
Shear strength [MPa]	35	30	30

Table 3. CF GG206P and CF GG90P (bidirectional carbon cloth with LG700 resin)

Parameter	X	Y	Z
Young modules [GPa]	57	57	10
Poisson ratio	0.25	0.25	0.25
Shear modules [GPa]	3.5	20	20
Density [kg/m^3]		1500	
Tensile strength [MPa]	640	640	65
Compressive strength [MPa]	495	495	120
Shear strength [MPa]	50	30	30

Table 4. The properties of TCU 330 (carbon fibre, unidirectional with LG700 resin)

Parameter	X	Y	Z
Young modules [GPa]	110	7.8	7.8
Poisson ratio	0.25	0.25	0.25
Shear modules [GPa]	5.9	1.5	1.5
Density [kg/m^3]		1600	
Tensile strength [MPa]	1600	55	55
Compressive strength [MPa]	1150	120	120
Shear strength [MPa]	50	30	30

kG (1 kG=9.80665 N). Additionally, the computational model was tilted by 1.35° to obtain the load component in the x-axis.

The results of the numerical calculations are presented in the following figures, showing displacements (Figure 9), stress distributions (Figure

Table 5. HEREX C70.55 (PVC foam)

Parameter	Parameter
Young modules [MPa]	45
Poisson ratio	0.31
Shear modules [MPa]	22
Density [kg/m^3]	60
Tensile strength [MPa]	1.3
Compressive strength [MPa]	0.9
Shear strength [MPa]	0.8

10), deformations in the principal directions (Figure 11), stresses (Figure 12) and deformations (Figure 13) at the most stressed points of the structure, as well as stresses and deformations in the individual layers of the most stressed part of the structure.

Results of numerical analyses:

The maximum deflection of the wing tips in the Z direction is 87.59 mm. Displacements in the X and Y directions are insignificant. The maximum deformations in the Y direction exceed 1% locally. The areas where this value has been exceeded are the area of the connection between the wings and the fuselage, on the upper and lower coverings. The deformations in the X direction are a maximum of 0.8% and are in the same region as the maximum deformations in the Y direction. The maximum stresses in the Y direction in the model are on the lower girder belt (stress along the fibre direction) of 509 MPa. In aerospace structures, a safety factor of 1.5 is commonly applied. Based on the performed numerical analyses, the maximum stress occurring within the investigated structure was determined to be 509 MPa. As the failure criterion, the ultimate strength of the TCU 330 carbon fibre composite (unidirectional configuration) with LG700 resin was adopted, with a tensile strength of 1150 MPa.

After applying the safety factor of 1.5, the allowable stress level for the structure is equal to 767 MPa. Therefore, the maximum stress obtained from the numerical analysis remains significantly below the allowable limit. Consequently, the most highly loaded structural component exhibits a strength margin exceeding 258 MPa, confirming that the analysed structure satisfies the assumed strength requirements. According to the analyses, it can be concluded that the structure will withstand the given loads provided for in the strength test at point D of the load envelope, because the allowable stress limit is not reached.

The investigated structure was subjected to the design load cases representative of

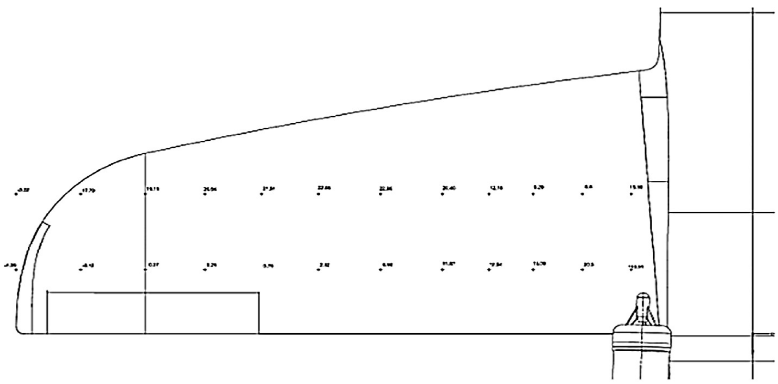

Figure 7. Forces acting on the wing

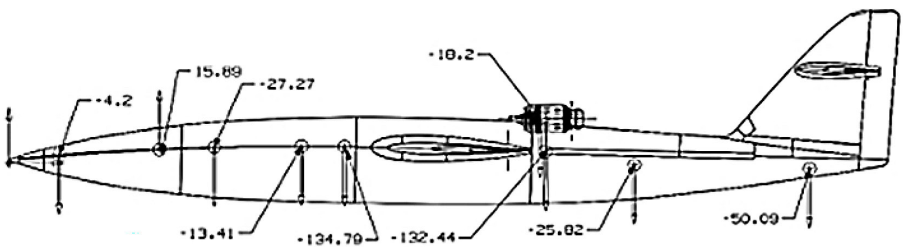

Figure 8. Forces acting on the fuselage

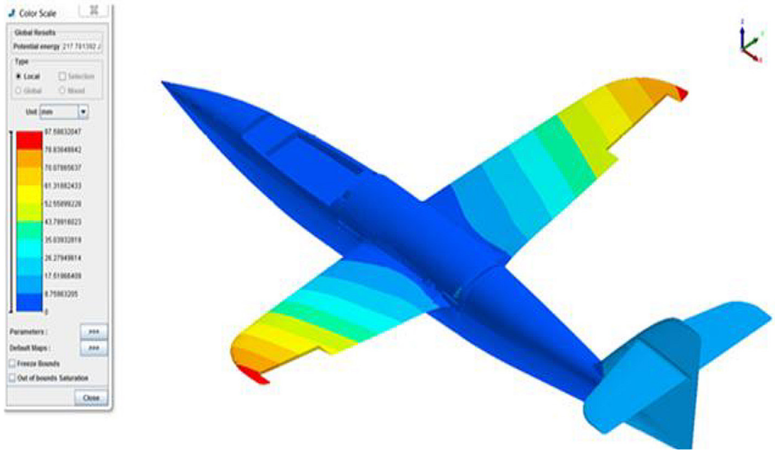

Figure 9. Displacements in the computational model

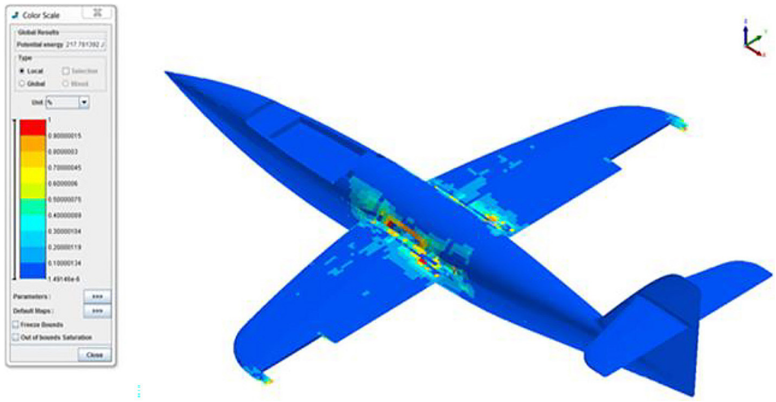

Figure 10. Strain along the fibres

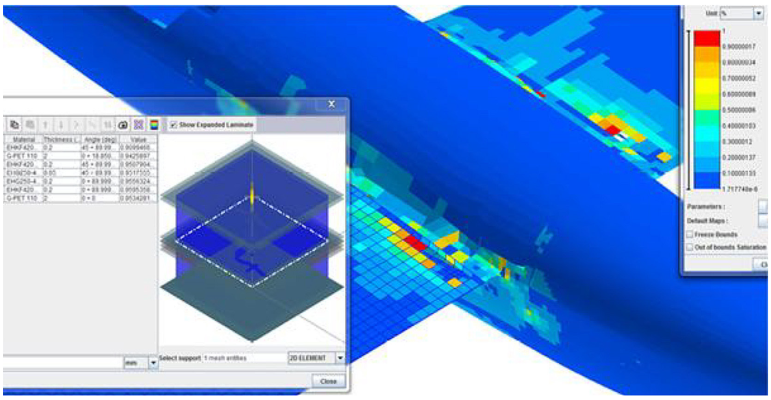

Figure 11. Strain in the fibre direction and in the most stressed components

operational conditions. Attention was given to the regions commonly associated with elevated stress concentrations, including fastener holes, cut-outs, geometric transitions, and areas of load introduction. A high-fidelity finite element model was employed to accurately capture local stress gradients and the complex stress distribution in the vicinity of these structural features.

The analysis revealed that stress concentrations occur primarily near geometric discontinuities, where load paths are locally disturbed, resulting in increased stress levels relative to the surrounding structure. The highest stress values were observed in the vicinity of load-transfer regions and local changes in structural stiffness. Despite the presence of localised stress peaks,

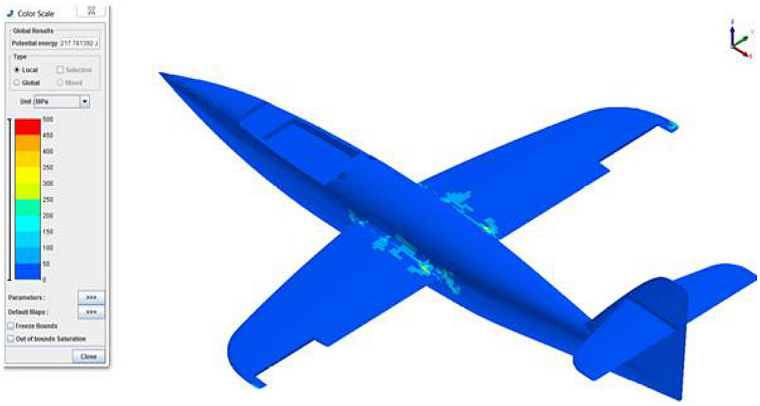

Figure 12. Stresses along the fibres

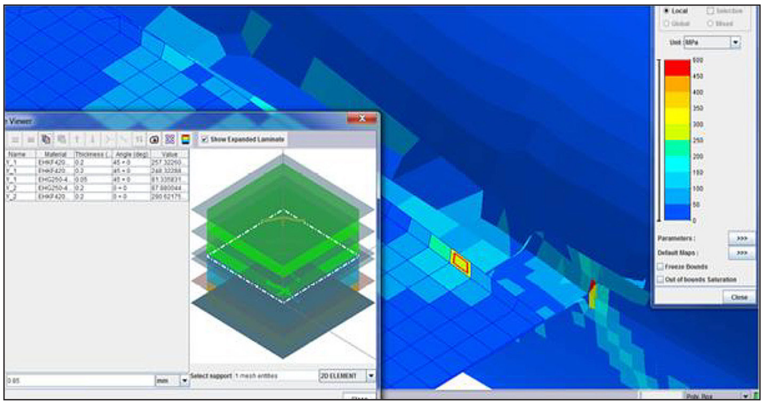

Figure 13. Stress on the direction of the fibres in the most stressed layers

the calculated stresses remained below the allowable limits established by the adopted material properties and safety requirements. The obtained results indicate that the structural design provides an adequate load-carrying capability while maintaining acceptable stress levels in critical regions.

The results demonstrated that the critical buckling loads exceed the design load levels, indicating that the structure possesses an adequate margin of safety against instability. No significant global or local buckling phenomena were predicted within the operational load range. Therefore, the analysed structure satisfies the applicable stability requirements and is expected to maintain its load-carrying capability without experiencing instability-induced failure.

Overall, the assessment confirms that the structural configuration provides sufficient resistance to buckling and that the design is suitable for the intended aerospace application. Such analyses constitute an essential part of the structural verification process, ensuring that both strength and stability requirements are satisfied throughout the operational envelope.

To improve durability, it was recommended to stiffen the structure in the area of the connection between the horizontal and vertical tails, as well as around the connection between the wings and the fuselage.

Ground static tests

The ground static test allows analysing the structural integrity of an aircraft without leaving the ground. This is a valuable part of the testing process that helps speed up the certification process, as it does not require a fully functional and completed aircraft [43-48]. A similar test has been performed for the cited in introduction [10] the General Atomics MQ-9B airframe at the Wichita State University's National Institute for Aviation Research [49].

According to CS-VLA regulations, the static ground tests of the aircraft were performed on a specially designed stand-up rig (Figure 14) for three main cases:

1. Wings and fuselage, pull-out diving speed, at point D (Figure 3).

2. Fuselage and horizontal tail - brutal steering, at V_A speed.
3. Fuselage and vertical tail - flight of the aircraft with slide (13°), at V_A speed.

The test station (Figure 14) consisted of a support frame made of high-strength steel profiles, a system of weights or hydraulic actuators (simulating the external load), sensors and force transducers. Cables, pulleys, and winches were stretched throughout the installation and used to precisely position, manipulate, or measure the behaviour of the examined object (OCP) in response to the forces given (load). The OCP was mounted in the centre of the frame (Figure 14).

Aerodynamic and mass loads in static wing tests were introduced in the form of a set of concentrated forces distributed along the span in two lines: the front and rear spar. Since the tests assumed the application of loads to the wing in the form of clamps, on the last section of the wing, on the intersection of the front spar and the clamp, the point of application of the force was introduced. In the fuselage, mass forces were introduced with weights hung on stickers and the engines were replaced with a dummy made of wood. The forces on the tails were introduced by means of clamps; The point of application of the force on the clamp was changed each time depending on the position of the resultant force on the tail. Figure 15 shows the OCP aircraft ready for testing and the loading system, simulating the loads on the wings and horizontal tail. The load was simulated with a hydraulic actuator and measured with a dynamometer. The load was applied to the wing, whereas reactions were introduced through the fuselage to the frame of the rig.

The test was carried out for 100% of the permissible loads. After loading up to 20% of the maximum loads, the inspection of the wing showed only deflection, without plastic deformations and damages. The possibility of tilting the ailerons to 100% of the allowed load was checked. The ailerons are tilted to the full extent without jamming. During the tests, no deflections, deformations, or stresses were measured, but the OCP structure was tested using Dantec Q800 and Q810 nondestructive testing systems [50, 51]. The Q800 series (Laser Shearography System) is a portable and compact measuring system for non-contact and non-destructive inspection of a material. The system is suited for inspection of complex materials and material combinations, i.e. composites, such as fibre-reinforced plastics, honeycomb structures, glare, etc. Non-destructive testing showed no damage to the OCP airframe.

Similar tests (Figure 16) were performed for the fuselage and horizontal tail (brutal steering, at V_A speed, and fuselage and horizontal tail (flight of an aircraft with a slide (13deg), at V_A speed); the result of the tests was also positive – no damage.

Static test results

Static tests on the ground did not indicate any damage or deformation to the airframe. In the case of the wing and fuselage, after relieving up to 20% of the permissible loads, the comparison of the wing deflections did not show any deformations. The possibility of tilting the ailerons to 100% of the allowed load was checked; the ailerons were fully operated without jamming. The non-destructive method of the Dantec Q800 and Q810 systems confirmed structural integrity of the OCP airframe.

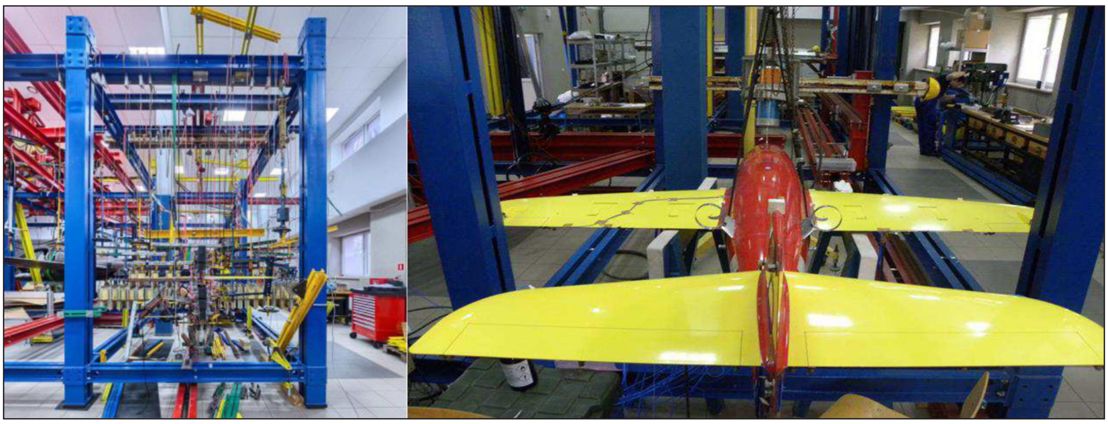

Figure 14. The measuring station (up) and the OCP airframe mounted in the rig (below)

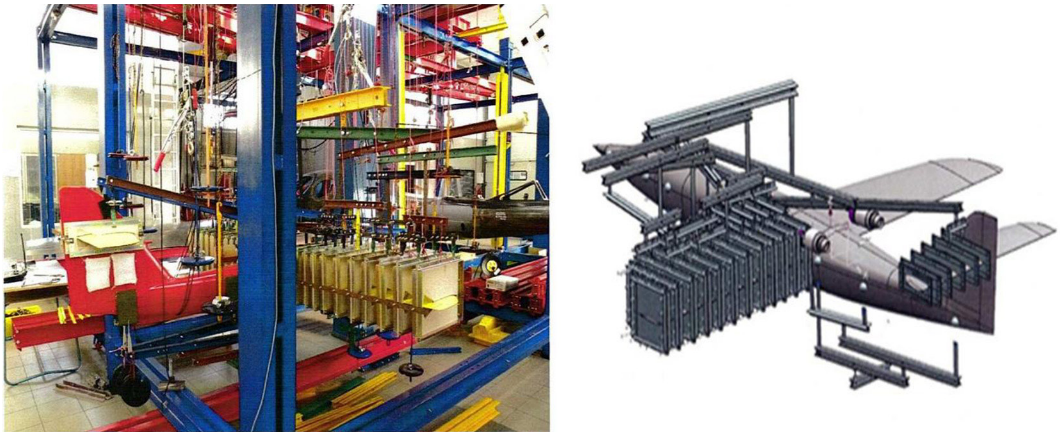

Figure 15. OCP airframe during testing and loading system

Figure 16. The OCP during fuselage and tail tests (horizontal and vertical) and the loading system (CAD model)

The static test was performed to obtain system certification (by the Military Aviation Authority) and there was no need to determine the structure deviation or displacement. During the static test, the structure was required to remain intact under the load prescribed by the certification procedure, with no occurrence of structural failure.

CONCLUSIONS

Based on the results of numerical analyses, it can be concluded that the structure will withstand the specified loads provided for in the strength test at the critical points of the load envelopes. Destructive values of deformations and stresses are only exceeded in points. However, to improve durability, it was recommended to stiffen the structure around the connection of the horizontal and vertical tails, as well as in the area of connection of the wings with the fuselage.

Static tests confirmed the results of numerical analyses and did not show any damage or plastic deformation of the airframe. During the strength tests, the OCP structure withstands the given loads.

The force structure of the OCP airframe has successfully passed the tests and qualifies it for certification according to the European airworthiness regulations CS – VLA (very light aircraft) and accepted by the Military Aviation Authority as the airworthy system.

Both methods confirmed that the strength requirements are met by the designed aircraft. Moreover, it was confirmed by the aircraft's flight qualification tests at the Polish Air Force training range. In this way, errors and design corrections were avoided. The experience acquired by the team is used to design a new, both simple and complex aircraft in accordance with the requirements of EASA CS 23 and CS 25.

REFERENCES

1. Taylor, J., Jane's All the World's Aircraft 1982–83. London, England: Jane's Yearbooks, 1982.
2. Leversedge, T., Canada Aviation and Space Museum aircraft Ryan KDA-4 Firebee drone RCAF Serial KD-4788 (PDF). Ottawa, Ontario: Canada Aviation and Space Museum. Archived from the original (PDF) on 2021-11-22. Retrieved 2020-11-05.
3. Wagner, W., Lightning Bugs and other Reconnaissance Drones, Aero Publishers Inc., Fallbrook, CA, USA, 1982; 85–91.
4. Janes All the World's Aircraft: In Service 2024–2025 yearbook.
5. Janes All the World's Aircraft: Development & Production 2024-2025 yearbook.
6. Strembski, M., War over Ukraine, Aviation, 2024; 1: 32–39.
7. Jayakrishna, K., Kar. V., Sultan, M., Rajesh, M., Sustainable composites for aerospace applications, Woodhead Publishing Series in Composites Science and Engineering, 2018; 1–18. https://doi.org/10.1016/B978-0-08-102131-6.00001-3
8. Hairi, S., Saleh, S., Ariffin, A., Omar, Z., A review on composite aerostructure development for UAV application, Composites Science and Technology, 08 July 2023; 137–157.
9. Yilmaz, A., Hasirci, K., Gündüz, B., Advanced composite wing design for next-generation military UAVs: A progressive numerical optimization framework, Defence Technology, June 2025; 48: 141–155. https://doi.org/10.1016/j.dt.2025.02.020
10. General Atomics Aeronautical Systems, Inc. (GA-ASI) https://www.ga.com/unmanned-aircraft-systems-and-sensors
11. Collective work – Zalewski, P. (project manager); Strength analysis of the structure of the "OCP" jet aerial target, Report of the project entitled "Jet aerial targets with programmed flight path", Contract No. DOBR/0065/R/ID1/2012/03, Military University of Technology, Warsaw, 2018.
12. Rykaczewski, D., Jastrzębski,. G., Szczepaniak. P., Sibilski K. Methodology for conducting preliminary and state tests of an aerial jet target set. Journal of KONBiN; 2020; 50(1): 2023. https://doi.org/10.2478/jok-2020-001
13. Frant M., Kiszkowiak Ł., Majcher M., Zalewski P.; Experimental tests and numerical analysis of aerodynamic properties of the composite-made Jet-propelled Aerial Target, MDPI – Materials 2024; 17(14): 3575. https://doi.org/10.3390/ma17143575
14. Chachurski R., Omen Ł., Panas A. J., Zalewski P. Mobile engine test station for preparation and operation of miniature turbine jet engines for flying aerial targets, Bulletin of Military University of Technology, 2020; 69(4). https://doi.org/10.5604/01.3001.0015.3819
15. Chachurski R., Omen Ł., Panas J. A., Zalewski P.; Ground testing of a miniature turbine jet engine with specific flight conditions, MDPI Energies 2025; 18(1): 73. https://doi.org/10.3390/en18010073
16. European Aviation Safety Agency - Certification Specifications for Very Light Aircrafts CS-VLA
17. Federal Aviation Administration, Department of Transportation, Code of Federal Regulations. Aeronautics and Space 14. Parts 1 to 59. Chapter I -Federal Aviation Administration, Department of Transportation. Subchapter C - Aircraft. Published by the Office of the Federal Register National Archives and Records Administration USA January 1994.
18. Etkin, B., Dynamics of Atmospheric Flight. John Wiley & Sons, Inc. 1972.
19. Taylor, J., Manual on Aircraft Loads. Pergamon Press.
20. Chun-Yung Niu M. Airframe Structural Design. Second Edition, Hong Kong Conmilit Press Ltd., 1999.
21. Howe D. Aircraft Loading and Structural Layout. AIAA Education Series, April 26, 2004.
22. Donaldson B. K. Analysis of Aircraft Structures – An Introduction. Second Edition, Cambridge Aerospace Series, 2008.
23. Albuquerque, P., Cunha, F. S., Reis L., Evaluation of Structural Loads. Conference: 3rd Aircraft Structural Design Conference, Royal Aeronautical Society At: Netherlands, October 2014.
24. Jang, J. H., Sang, H. A., FE modelling methodology for load analysis and preliminary sizing of aircraft wing structure. International Journal of Aviation, Aeronautics and Aerospace, 2019; 6(2), 1.
25. Michael C. Y., Composite Airframe Structures, Commit Press Ltd., Los Angeles, 1992.

26. Chung, D. L., Carbon Fiber Composites, Butterworth-Heinemann, Boston, 1994.
27. Baker, A., Dutton, S., Kelly, D., Composite Materials for Aircraft Structures, American Institute of Aeronautics and Astronautics, Reston, 1996.
28. Jones, R. M., Mechanics of Composite Materials, Virginia Polytechnic Institute and State University, Blacksburg, 1999.
29. Roylance, D., Introduction to Composites, Massachusetts Institute of Technology, Cambridge, 2000.
30. Soutis, C. Fiber reinforced composites in aircraft construction. Prog. Aerosp. Sci. 2005; 41: 143–151.
31. Taylor, R.P. Fiber Composite Aircraft—Capability and Safety; Australian Transport Safety Bureau: Canberra, Australia, 2008.
32. Beukers, A., Bersee, H., Koussios, S., Future Aircraft Structures: From Metal to Composite Structures. In Composite Materials - A Vision for the Future; Springer: London, UK, 2011.
33. Arkuszyński, P., Rośkowicz, M., Influence of Preloading on Damage in CFRP Composite Material Subjected to Low-Energy Impact Loads, MDPI Materials 2025; 18(17): 4016.
34. Xu, X., Peng, G., Zhang, B., Shi, F., Gao, L., Gao, J., Material performance, manufacturing methods, and engineering applications in aviation of Carbon fiber reinforced polymers: A comprehensive review. Thin-Walled Struct. 2025; 209: 112899.
35. Korba, P. Al-Rabeei, S., Hovanec, M., Sekelová, I., Kale, U., Structural design and material comparison for aircraft wing box beam panel. Heliyon 2024; 10: e27403.
36. Zhang, J., Lin, G., Vaidya, U., Wang, H., Past, present and future prospective of global carbon fibre composite developments and applications. Compos. Part B Eng. 2023; 250: 110463.
37. Pezzuti, E., Donnici, G., Structural composites for aircraft design. J. Eng. Appl. Sci. 2014; 9: 1889–1898. [Google Scholar]
38. Arkuszyńska, A., Rośkowicz, M., Effect of elevated temperature on load-bearing capacity and fatigue life of bolted joints in CFRP components. MDPI Polymers 2026; 18(2): 182.
39. Saxena, A., Sahay, B. Computer Aided Engineering Design, Springer – Anamaya, 2005.
40. Jiapeng, T., Ping, X., Baoyuan, Z., Bifu, H., A finite element parametric modeling technique of aircraft wing structures. Chinese Journal of Aeronautics, October 2013; 26(5): 1202–1210.
41. Rabbey F., Rumi, M., Nuri, H., Monerujjaman, H., Hassan M., Structural deformation and stress analysis of aircraft wing by finite element method. Advanced Materials Research April 2014; 906: 318–322.
42. Olejnik, A., Zalewski, P., Kiszkowiak, Ł., Rogólski, R., Finite element analysis of the suspended satellite rocket weight effect on the strength and deformability of the MiG-29 aircraft structure, proceedings of the institution of mechanical engineers, part G, Journal of Aerospace Engineering, 2023; 0(0): 1–19, https://doi.org/10.1177/09544100231189942
43. Boggs, B., C., The history of static test and air force structures, technical report AFFDL-TR-79-307I, 1979.
44. Acar, E., Hafka, R.T., and Kim N.H. Effects of structural tests on aircraft safety. AIAA Journal, 2010; 48: 2235–2248.
45. Mares C., Ursache N., Aircraft Ground Structural Testing. 2014. https://doi.org/10.1002/9780470686652.eae610
46. Flight Global, Boeing completes 787 ultimate-load wing flex tests. http://www.flightglobal.com/news/articles/picture-boeing-completes-787-ultimate-load-wing-flex-340014/ (accessed Jan 14, 2014).
47. Wright, J., Cooper J., Introduction to Aircraft Aeroelasticity and loads, Second Edition, Wiley&Sons Ltd., 2015.
48. Gates, D., Boeing & Aerospace, Newsletter, Boeing 777X's fuselage split dramatically during September stress test, Nov. 27, 2019.
49. NIAR wraps up structural testing for MQ-9B aircraft, Composite World, Published 12/01/2025, https://www.compositesworld.com/news/niar-wraps-up-structural-testing-for-mq-9b-aircraft
50. Dantec Dynamics, https://www.dantecdynamics.com
51. Dantec Dynamics Q 800 Automated Shearography Robosystem, https://www.youtube.com/watch?v=t6IGP0skQb8